Blockage effects on viscous fluid flow and heat transfer past a magnetic obstacle in a duct*

Zhang Xi-Dong(张喜东) and Huang Hu-Lin(黄护林)†

Academy of Frontier Science, Nanjing University of Aeronautics and Astronautics, Nanjing 210016, *China*

(Received 11 October 2012; revised manuscript received 24 December 2012)

The effect of lateral walls on fluid flow and heat transfer is investigated when a fluid passes a magnetic obstacle. The blockage ratio β that represents the ratio between the width of external magnet M_y and the spanwise width L_y is employed to depict the effect. The finite volume method (FVM) based on the PISO algorithm is applied for the blockage ratios of 0.2, 0.3, and 0.4. The results show that the value of Strouhal number St increases as the blockage ratio β increases, and for small β, the variation of St is very small when the interaction parameter and Reynolds number are increasing. Moreover, the cross-stream mixing induced by the magnetic obstacle can enhance the wall-heat transfer and the maximum value of the overall heat transfer increment is about 50.5%.

Keywords: magnetic obstacle, blockage ratio, strouhal number, heat transfer

PACS: 52.30.Cv, 44.27.+g, 47.32.cb **DOI:** 10.1088/1674-1056/22/7/075202

1. Introduction

A large amount of work in the literature has been devoted to the study of liquid metal flow in a duct with a uniform transverse magnetic field because of its application to important technologies,[1–5] such as the new generation of fusion reactors (Tokamaks).[6] However, the flow past a local magnetic field distribution is a rather new magnetohydrodynamic (MHD) problem that is not yet well understood qualitatively. The non-uniform magnetic field exists widely in many important technologies such as crystal growth processes and electromagnetic stirring and mixing.[5,7] Gelfgat *et al.*[8] first performed two-dimensional numerical calculations about the liquid metal flow around a local magnetic field and found two vortices inside the magnetic field region. However, Gelfgat and Olshanskii[9] have not confirmed the numerical finding in especially experimental studies. Recently, Cuevas *et al.*[10] analyzed numerically quasi-two-dimensional flow past a local magnetic field at low Reynolds numbers 100 and 200, and the Reynolds number (Re) is defined as $Re = UL/\nu$, where U is the bulk horizontal inlet velocity, L is the vertical half-distance of the rectangular duct (in the z direction), and ν is the kinematic viscosity. They introduced the term "magnetic obstacle" to describe the flow which could exhibit some features similar to those observed in ordinary hydrodynamics of fluid flow around a circular cylinder and discovered that vortex shedding occurred in the wake of the magnetic obstacle with the Hartmann number increasing. The Hartmann number represents a ratio between the Lorentz and viscous forces, $Ha = B_0 L\sigma^{1/2}/(\rho\nu)^{1/2}$, where B_0 is the magnetic field intensity in the center of the magnetic gap, σ and ρ are the electric conductivity and the density of the fluid, respectively. Three-dimensionl numerical and experimental results of Votyakov *et al.*[11] indicated that stable six-vortex structures were formed at high Reynolds numbers. Votyakov and Kassinos[12] reported the analogy between an electrically conductive fluid flow through a magnetic obstacle and the ordinary hydrodynamic flow around a solid obstacle. They showed that the breaking away of attached vortices from the magnetic obstacle was similar to that occurring past a solid obstacle. Kenjeres *et al.*[13] investigated numerically the vortical structures and turbulent bursts behind a magnetic obstacle in transitional flow regimes. The Reynolds number ranges $10 \leq Re \leq 900$ for different values of the magnetic interaction parameters $(4, \ldots, 25)$ were considered in their investigation. The magnetic interaction parameter N represents the ratio between the Lorentz and inertial forces, i.e., $N = Ha^2/Re$. The results revealed that the turbulence was sustained locally in the proximity of the magnetic wake edge. And the rapid turbulence decay indicated that the flow will fully relaminarise farther downstream. However, the works mentioned above did not report the heat transfer characteristics of electrically conducting fluid past a magnetic obstacle and the effect of the blockage ratio on the fluid flow and the heat transfer. In this work, we further extend the above investigation to a three-dimensional duct, and study the effect of the blockage ratio on the vortex structures, vortex shedding frequency, and wall-heat transfer at different interaction parameters and Reynolds numbers.

*Supported by the National Natural Science Foundation of China (Grant No. 51176073), the Specialized Research Fund for the Doctoral Program of Higher Education of China (Grant No. 20103218110027), and the Priority Academic Program Development of Jiangsu Higher Education Institutions (PAPD), China.

†Corresponding author. E-mail: hlhuang@nuaa.edu.cn

© 2013 Chinese Physical Society and IOP Publishing Ltd

2. Mathematical formulation

2.1. Governing equations and boundary conditions

The physical model is shown in Fig. 1, with the length $L_u + L_d = 0.75$ m, width $L_y = 0.1$ m, 0.1334 m and 0.2 m, and height $H = 0.02$ m. To depict the effect of a lateral wall, the blockage ratio β is defined as $\beta = M_y/L_y$, here, M_y is the width of external magnet. The duct is filled with the eutectic alloy GaInSn with Prandtl number $Pr = 0.020$. The external magnets with the following sizes: $(M_x, M_y, h) = (0.03$ m, 0.04 m, 0.03 m) are assembled symmetrically on the top and bottom walls that lay along the z direction, and the magnitude can be calculated by a semianalytical simplification of the Biot–Savart and Maxwell equations[11,13]

$$B_{0x}(x,y,z) = \gamma \sum_{k=\pm1}\sum_{j=\pm1}\sum_{i=\pm1}(ijk)\operatorname{artanh}\left[\frac{y-0.5jM_y}{r(i,j,k)}\right], \quad (1)$$

$$B_{0y}(x,y,z) = \gamma \sum_{k=\pm1}\sum_{j=\pm1}\sum_{i=\pm1}(ijk)\operatorname{artanh}\left[\frac{x-0.5iM_x}{r(i,j,k)}\right], \quad (2)$$

$$B_{0z}(x,y,z) = -\gamma \sum_{k=\pm1}\sum_{j=\pm1}\sum_{i=\pm1}(ijk) \times \arctan\left[\frac{(x-0.5iM_x)(y-0.5jM_y)}{(z-0.5kh)r(i,j,k)}\right], \quad (3)$$

where

$$r(i,j,k) = \left[(x-0.5iM_x)^2 + (y-0.5jM_y)^2 + (z-0.5kh)^2\right]^{1/2},$$

and the external magnetic field B_0 is obtained in such a way that $B_{0z}(0,0,0) = B_0$, and the center of the magnetic gap is the center of the coordinate system.

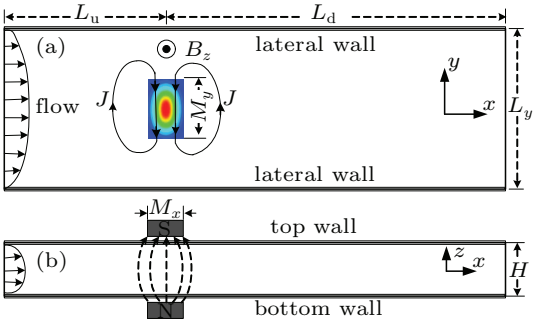


Fig. 1. (color online) Sketch of physical domain: (a) top (x–y plane) view; and (b) side (x–z plane) view.

Some assumptions are made in our model as follows: (i) the fluid is an incompressible Newtonian fluid; (ii) the flow is laminar flow; (iii) all the walls are electrically insulating. In this case, the dimensionless MHD equations of continuity, momentum, and energy reduce to

$$\nabla \cdot \boldsymbol{u}^* = 0, \quad (4)$$

$$\frac{\partial \boldsymbol{u}^*}{\partial t^*} + (\boldsymbol{u}^* \cdot \nabla)\boldsymbol{u}^* = -\nabla p^* + \frac{1}{Re}\nabla^2 \boldsymbol{u}^* + N(\boldsymbol{J}^* \times \boldsymbol{B}^*), \quad (5)$$

$$\frac{\partial \Theta}{\partial t^*} + (\boldsymbol{u}^* \cdot \nabla)\Theta = \frac{1}{Pe}\nabla^2 \Theta, \quad (6)$$

where the velocity $\boldsymbol{u}$, the pressure p, the electric current density $\boldsymbol{J}$, and the magnetic field $\boldsymbol{B}$ are normalized by U, ρU^2, $\sigma U B_0$, and B_0. The temperature is defined as $\Theta = (T - T_\infty)/(T_w - T_\infty)$, T_∞ and T_w are free stream temperature and side-wall temperature, respectively, $Re_m = \mu_m \sigma U L$ is the magnetic Reynolds number and $Pe = RePr$ is the Pelect number. Dimensionless coordinates x, y and z are all normalized by $L = H/2$, while time t is normalized by L/U. Here, μ_m and σ are the magnetic permeability and the electrical conductivity of the fluid, respectively. The induced magnetic field equation can be derived from Maxwell's equations and Ohm's law in MHD approximation[15]

$$\frac{\partial \boldsymbol{b}^*}{\partial t^*} + (\boldsymbol{u}^* \cdot \nabla)\boldsymbol{B}^* = \frac{1}{Re_m}\nabla^2 \boldsymbol{b}^* + (\boldsymbol{B}^* \cdot \nabla)\boldsymbol{u}^*, \quad (7)$$

where $\boldsymbol{B}^*$, the magnetic field intensity, is composed by the applied magnetic field $\boldsymbol{B}_0^*$ and the induced magnetic field $\boldsymbol{b}^*$. The applied magnetic field $\boldsymbol{B}_0^*$ satisfies the magnetostatic equations,[10,14] namely

$$\nabla \cdot \boldsymbol{B}_0^* = 0 \quad \text{and} \quad \nabla \times \boldsymbol{B}_0^* = 0. \quad (8)$$

Hence, the induced field implicitly satisfies

$$\nabla \cdot \boldsymbol{b}^* = 0, \quad (9)$$

which can be used to calculate the electric currents, $\boldsymbol{J}^* = (1/Re_m)\nabla \times \boldsymbol{b}^*$.

The walls are impermeable, electrically insulating, and no-slip. The inflow boundary condition at $x = -L_u = -0.25$ m is a symmetrical fully developed streamwise velocity with other velocities being set to zero. The temperature of the incoming stream and the temperature at the side wall ($y = -L_y/2$) are $\Theta = 0$ and $\Theta = 1$, respectively. The other walls are thermally insulated (a zero normal temperature gradient is imposed at its surface). The streamwise gradients of all variables such as the velocity and the temperature are set to zero at the outlet to satisfy the fully developed conditions.

Due to the fast decay of the external magnetic field, it has a high intensity only in a local zone which is assumed to be far from the inlet/outlet region as well as from the lateral boundaries at small β ($\beta = 0.2$). So the induced magnetic field is taken to be zero at $x = -L_u$, $x = L_d$, and $y = \pm L_y/2$. However, for large β ($\beta = 0.3$ and 0.4), the proper boundary conditions of the induced magnetic field at all the insulating walls can be expressed as $\boldsymbol{n} \cdot \boldsymbol{b} = 0$ and $\boldsymbol{n} \times \boldsymbol{b} = 0$. Here, $\boldsymbol{n}$ denotes the normal line of the boundary.[1,10]

2.2. Method of solution

The finite volume method based on the staggered grid system was used to discretize the governing equations in space. The discrete equations were solved by a fully implicit method in time marching and a second-order scheme was employed for the time integration. In the work the convective terms were discretized using the second-order upwind scheme while the

central difference approximation was applied to the diffusion terms. The pressure-implicit with splitting of operators (PISO) algorithm was employed for the pressure–velocity coupling for all simulations. The update would continues until the relative difference between two successive iterations satisfied the following criterion: $|\phi^{n+1} - \phi^n|/|\phi^n| \leq 10^{-6}$, where ϕ^n represents the dependent variable at the n-th iteration.

The numerical grid is regular and non-uniform with finer meshes in the regions near the magnetic obstacle edges and wall surfaces. The minimal horizontal step size in the region of the magnetic gap is $\Delta x = \Delta y = 0.25$. The characteristic thickness of the Hartmann layers is $\delta = H/Ha$.[3] There are 6-grid points in the boundary layer for present study, and the minimal vertical step size near the top and bottom (Hartmann) walls is $\Delta z = 0.005$. The calculations are repeated with a $150 \times 100 \times 80$ grid. We believe that the grid number is sufficient for the present simulation by comparison with the simulation of Votyakov *et al.*[12] All the computations are performed using 6 CPUs on the local Beowulf-Linux cluster.

3. Results and discussion

3.1. Validation of the numerical system

The code based on the FVM is extensively exercised to check its validity. In this paper, we present the code validation for three cases. The validation of the code is carefully performed by comparing our results with the published results obtained by Votyakov *et al.*[11] Figure 2(a) shows the comparion of streamwise velocity for three cases: CI-N=4, Re=100, CII-N=11.25, Re=100, and CIII-N= 11.25, Re=400. As can be seen, our results are more favourably graphically compared with those reported by Votyakov *et al.*[11] Further, a good qualitative agreement is found in terms of the vortex structures downstream of the magnetic obstacle, as shown in Figs. 2(b) and 2(c).

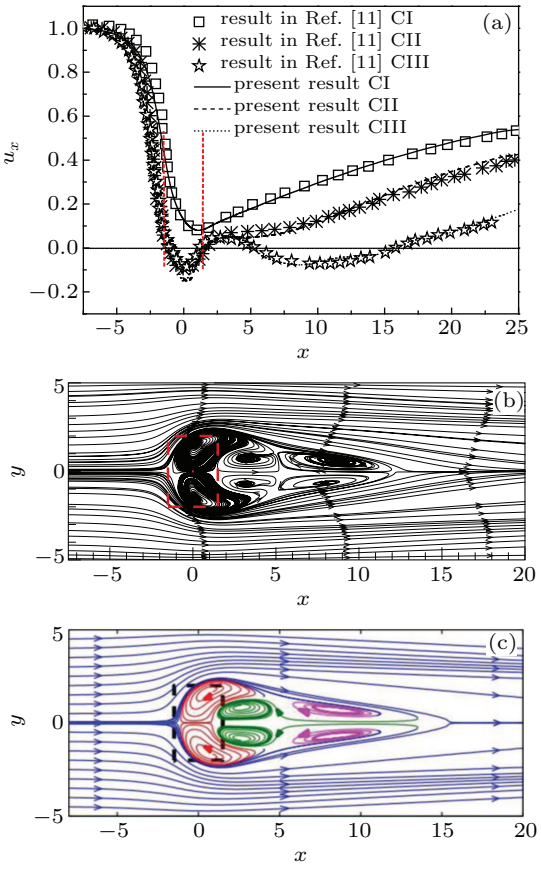


Fig. 2. (color online) (a) Streamwise velocitiy along the centerline ($z = 0$ and $y = 0$). (b) Wake structure of CIII in our simulations. (c) Wake structure of CIII obtained by Votyakov *et al.*[11] Dashed vertical lines mark borders of the external magnet.

3.2. Fluid flow

Figures 3(a)–3(c) and Figures 3(d)–3(f) show the instantaneous mass flow streamlines and the instantaneous contours of vorticity at different blockage ratios ($\beta = 0.2$, 0.3, and 0.4) at $Re = 900$ and $N = 15$. Contour levels are displayed between $-5 \leq \omega_z \leq 5$, with solid and dashed lines representing the positive and negative values of vorticity, respectively. As seen in Figs. 3(a)–3(c), the attached vortex comes off the magnetic obstacle and is carried by the underlying flow downstream away from the obstacle. This interesting behavior has also been observed by Votyakov *et al.*[12] The effect of the side wall is found to be negligible for a small blockage ratio ($\beta = 0.2$) because the side wall is far from the wake of magnetic obstacle, which causes the weak shear $\partial u/\partial y$ generated between the slowly moving core and accelerated the side jets. However, as the blockage ratio further increases from 0.2 to 0.4, the streamlines patterns near the walls are fluctuant, the connecting vortex pairs are unstable, and the vortex A accelerates shedding. This can be attributed to the strong shear $\partial u/\partial y$. Moreover, the shear increases as the blockage ratio increases since the mass conservation must be satisfied. For the instantaneous vorticity fields at $\beta = 0.2$, the wake consists of regular positive and negative vortices shed alternately from the shear layers either side of the magnetic obstacle. This behavior is also found at different Reynolds numbers and interaction parameters, which is not shown in this paper. As the blockage ratio further increases from 0.3 to 0.4, the flow behavior is completely dominated by the jets produced between the magnetic obstacle and the side boundary layers (Shercliff layers), and the produced flow becomes chaotic downstream, as shown in Figs. 3(e) and 3(f). Moreover, the flow interference between the shedding vortices and the Shercliff layers is quite strong at blockage ratio $\beta = 0.4$. Consequently, the oscillating regions are found to be more chaotic because the shedding vortices and jet have entrained fluid from the neighborhood and the Shercliff layers. This can be contributed to the short distance between the core region and the side walls transferring the shear easily at large blockage ratios.

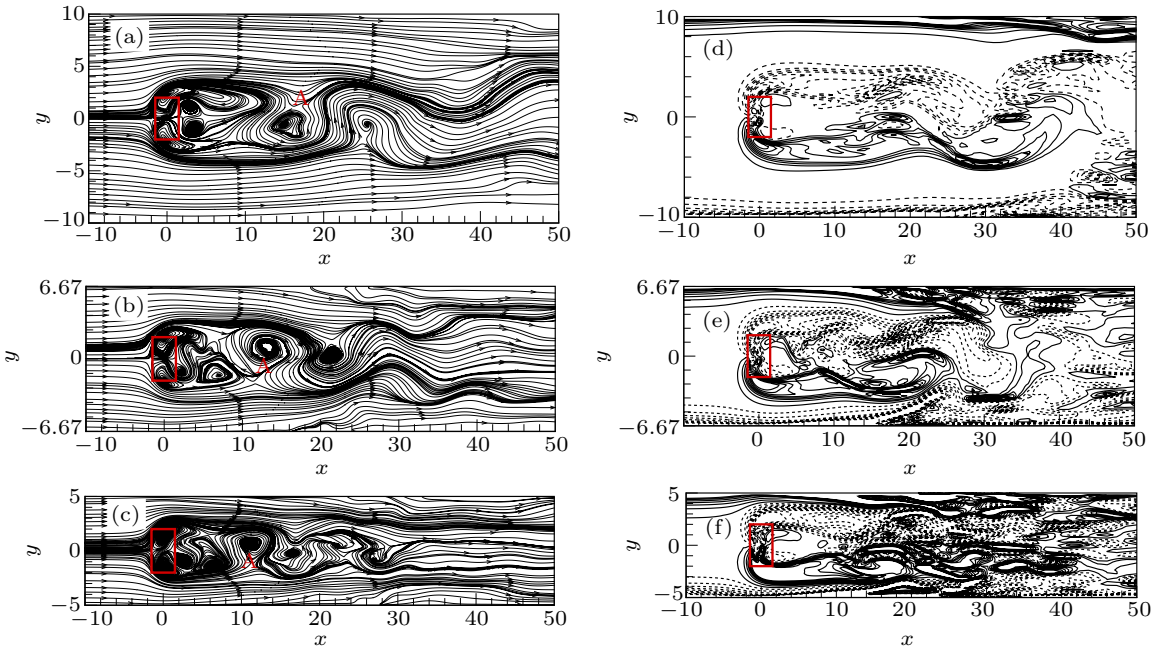


Fig. 3. (color online) Instantaneous mass flow streamlines (left) and the instantaneous contours of vorticity (right) with *Re*=900 and *N*=15 at different blockage ratios: (a) $\beta = 0.2$, (b) $\beta = 0.3$, (c) $\beta = 0.4$, (d) $\beta = 0.2$, (e) $\beta = 0.3$, (f) $\beta = 0.4$.

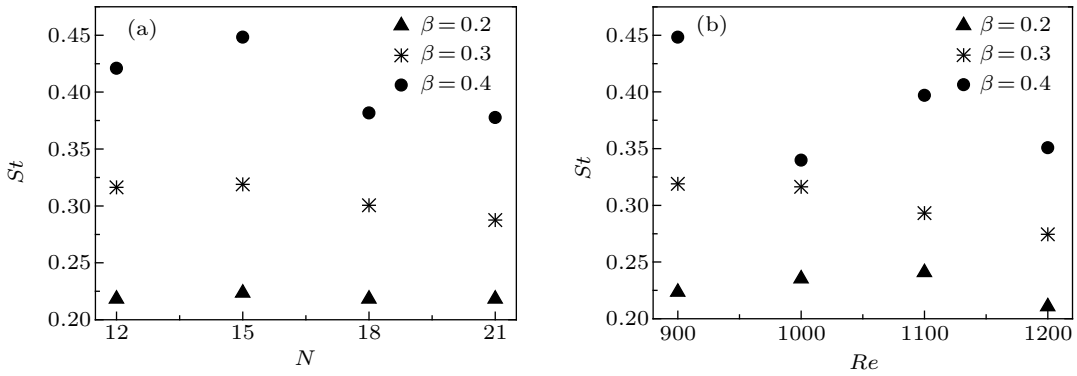


Fig. 4. Strouhal number plotted versus (a) *N* and (b) *Re* at different blockage ratios.

The vortex shedding frequency is an important quantity in the unsteady periodic flow, which is determined by the Strouhal number $St = fM_y/U$, where f is the fundamental frequency of vortex shedding. In this work, St is determined by fast Fourier transformation (FFT) of time traces of the spanwise component of velocity. Figure 4 illustrates the variation of St versus N and Re. For small β ($\beta = 0.2$), the frequency of vortex shedding is almost constant with N increasing. This phenomenon was observed by Kenjeres *et al.*[13] Similarly, for small β, the change of Strouhal number with the change of Reynolds number is small as shown in Fig. 4(b). However, as the blockage ratio increases further from 0.3 to 0.4, the change of Strouhal number is largely with N and Re changing, which shows that the effect of the lateral walls is important at large blockage ratios. Moreover, the Strouhal number increases with the increase of blockage ratio at constant interaction parameters and Reynolds numbers. Because the disturbance of the lateral walls accelerates the vortex shedding at large β.

3.3. Heat transfer

The distributions of instantaneous temperature contours for blockage ratios $\beta = 0.2$, 0.3, and 0.4 at N =15 and Re = 900 are shown in Fig. 5. From these figures, one can conclude that the increase of β benefits the heat transfer from the hot wall to the low-temperature fluid. The heat transfer is enhanced because the wake is chaotic. The thickness of the thermal boundary layer adjacent to the hot wall decreases with β increasing. For $\beta = 0.2$, the temperature field is characterized by a small vertical gradient of temperature across the duct because the flow is almost symmetrical, as can been seen from Figs. 3(a) and 3(d). Therefore, the presence of the magnetic obstacle has a small effect and does not grossly distort the temperature field in comparison with these cases in which the wake is chaotic at large blockage ratios ($\beta = 0.3$ and 0.4).

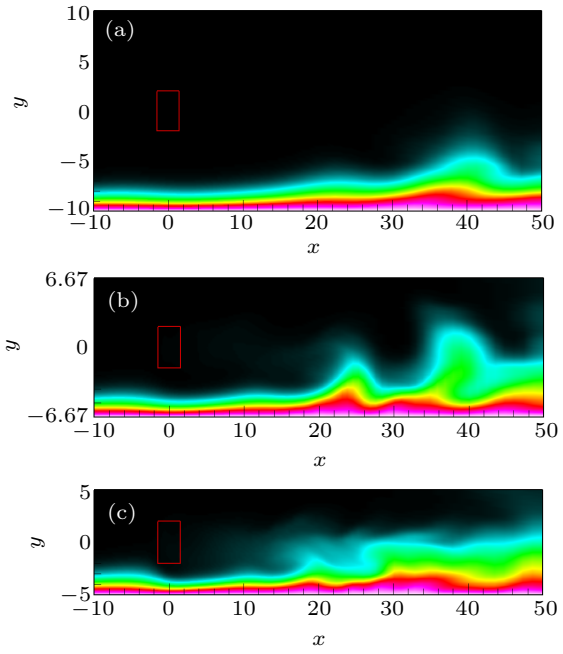


Fig. 5. (color online) Instantaneous temperature contours at Re = 900 and N =15 for (a) $\beta = 0.2$, (b) $\beta = 0.3$, and (c) $\beta = 0.4$. Light and dark shadings show hot and cold fluids, respectively.

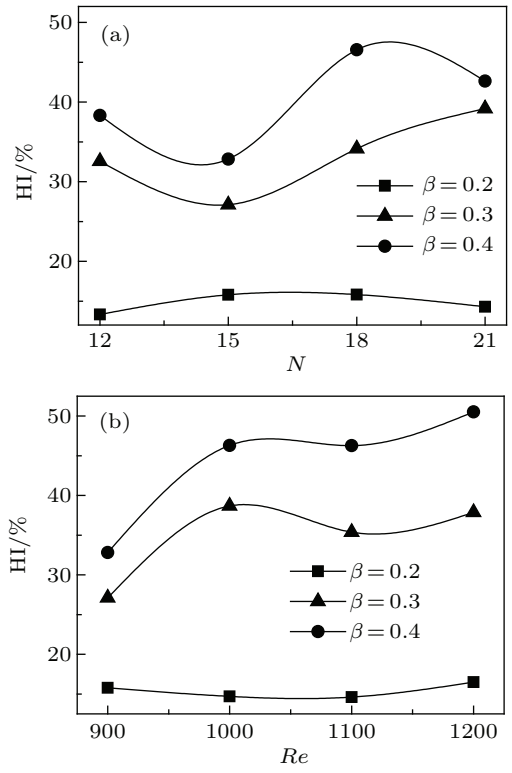


Fig. 6. The percentage increments of the overall heat transfer for different blockage ratios versus (a) N and (b) Re.

To characterize the effect on the heat transfer due to the magnetic obstacle, the total increment of heat transfer (HI) is defined as:

$$\mathrm{HI} = \frac{\langle \overline{Nu} \rangle - \langle \overline{Nu_0} \rangle}{\langle \overline{Nu_0} \rangle} \times 100\%,$$

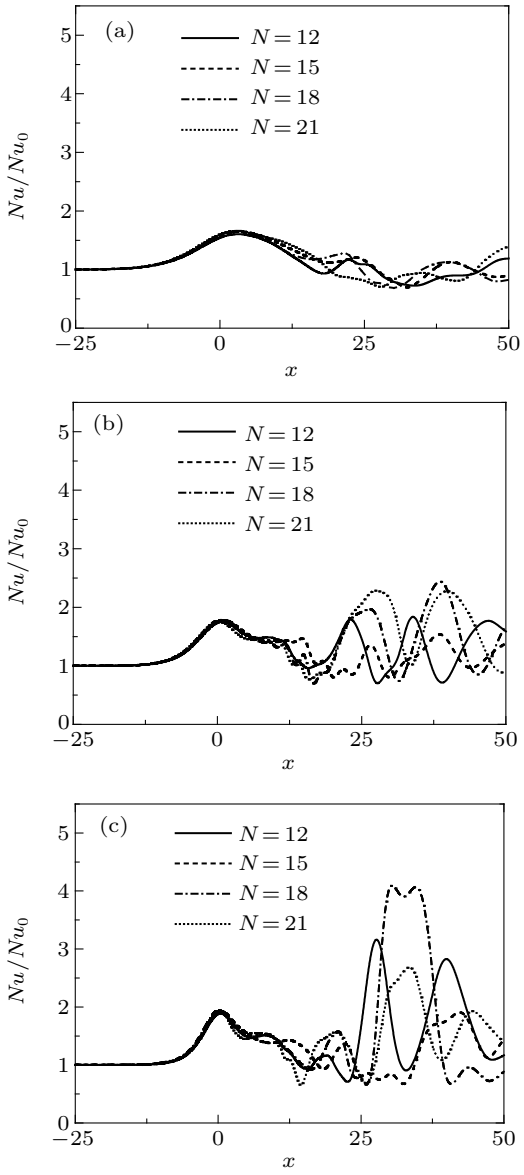


Fig. 7. Distributions of local Nusselt number Nu/Nu_0 along the hot wall for different blockage ratios: (a) $\beta = 0.2$; (b) $\beta = 0.3$; (c) $\beta = 0.4$.

where $\langle \overline{Nu_0} \rangle$ is the time and surface-averaged Nusselt number without the magnetic obstacle. The time- and surface-averaged Nusselt number

$$\langle \overline{Nu} \rangle = \frac{1}{\tau_p} \int_0^{\tau_p} \langle Nu \rangle \mathrm{d}t,$$

where $\langle Nu \rangle$ is the surface-averaged Nusselt number calculated by integrating the local Nusselt number Nu over the heated surface. The local Nusselt number

$$Nu = \frac{L}{(T_\infty - T_\mathrm{w})} \frac{\partial T}{\partial y} \Big|_{\mathrm{wall}}.$$

As shown in Fig. 6, the heat transfer is enhanced in all cases, and the increment is more pronounced at larger blockage ratios. The maximum value of the overall heat transfer increment is 50.5%. Local hot wall Nusselt number distributions Nu/Nu_0 for different blockage ratios and interaction parameters are shown in Fig. 7. The curves are also observed at

different Reynolds numbers (not shown here). In the inlet region, a thermally developing flow exists, and all curves show nearly identical behaviors because the flow is steady. When $x > 0$, the effect of the magnetic obstacle is very important for all blockage ratios (particularly between $\beta = 0.3$ and 0.4) because the periodic vortex shedding appears after the magnetic obstacle. In fact, the thermal boundary layer is greatly disturbed by the periodic flow caused by the magnetic obstacle, the high-temperature fluid near the hot region of the duct is removed far away and tends to be convected to the lateral wall ($y = +L_y/2$). Hence, the percentage increment is larger.

4. Conclusion

In this work, the effects of a magnetic obstacle on the fluid flow and heat transfer in a rectangular duct under various blockage ratios are investigated. The thermophysical properties of the fluid are assumed to be constant. As time goes on, the attached vortex comes off alternately the magnetic obstacle and is carried by the underlying flow in the streamwise direction. Moreover, The effect of the lateral walls on the fluid flow can be negligible when the blockage ratio $\beta \leq 0.2$. However, when $\beta > 0.2$, the side walls will strongly disturb the wake and cause the instability of connecting vortices pairs. Further, the side wall can accelerate the vortex shedding at large blockage ratios.

HI is increasingly dependent on the blockage ratio, and the value of HI increases as the blockage ratio increases at constant interaction parameters and Reynolds numbers. Moreover, at large blockage ratios ($\beta = 0.3$ and 0.4), the variation of the overall increment of the heat transfer with interaction parameter and Reynolds number is remarkable. And the maximum of HI is about 50.5% at N=15 and Re=1200.

Acknowledgment

The authors would like to thank the referees for their useful suggestions and comments for improving the original manuscript.

References

[1] Huang H L, Ying A and Abdou M A 2002 *Fusion Eng. Des.* **63** 361
[2] Salem A M and Fathy R 2012 *Chin. Phys. B* **21** 054701
[3] Ni M J, Munipalli R and Morley N B 2007 *J. Comput. Phys.* **227** 174
[4] Dousset V and Pothérat A 2008 *Phys. Fluids* **20** 017104
[5] Hussam W K, Thompson M C and Sheard G J 2011 *Int. J. Heat Mass Transfer* **54** 1091
[6] Jiang H B, Wang A K and Peng X D 2010 *Chin. Phys. B* **19** 115205
[7] Davidson P 1999 *Annu. Rev. Fluid Mech.* **31** 273
[8] Gelfgat Y M, Peterson D E and Shcherbinin E V 1978 *Magnetohydrodynamics* **14** 55
[9] Gelfgat Y M and Olshanskii S V 1978 *Magnetohydrodynamics* **14** 151
[10] Cuevas S, Smolentsev S and Abdou M A 2006 *J. Fluid Mech.* **553** 227
[11] Votyakov E V, Kolesnikov Y, Andreev O, Zienicke E and Thess A 2007 *Phys. Rev. Lett.* **98** 144504
[12] Votyakov E V and Kassinos S C 2009 *Phys. Fluids* **21** 097102
[13] Kenjeres S, Ten Cate S and Voesenek C J 2011 *Int. J. Heat Fluid Flow* **32** 510
[14] Votyakov E V, Kassions S C and Albert-Chico X 2009 *Theor. Comput. Fluid Dynam.* **23** 571
[15] Moreau R 1990 *Magnetohydrodynamics* (Dordrecht: Kluwer Academic Publishers) pp. 4–10